Serum glial fibrillary acidic protein correlates with retinal structural damage in aquaporin-4 antibody positive neuromyelitis optica spectrum disorder

Lin T.Y., Schindler P., Grittner U., Oertel F.C., Lu A., Motamedi S., Yadav S.K., Duchow A.S., Jarius S., Kuhle J., Benkert P., Brandt A.U., Bellmann-Strobl J., Schmitz-Hübsch T., Paul F., Ruprecht K., Zimmermann H.G.

This is the final version of the accepted manuscript. The original article has been published in final edited form in:

Multiple Sclerosis and Related Disorders
2022 NOV ; 67: 104100
2022 AUG 09 (first published online: final publication)
DOI: 10.1016/j.msard.2022.104100

Publisher: Elsevier

Serum glial fibrillary acidic protein correlates with retinal structural damage in aquaporin-4 antibody positive neuromyelitis optica spectrum disorder

Ting-Yi Lin*[1,2,3,4], Patrick Schindler*[1,2,3,5], Ulrike Grittner[6,7], Frederike C. Oertel[1,2,3,8], Angelo Lu[1,2,3,4], Seyedamirhosein Motamedi[1,2,3,4], Sunil Kumar Yadav[1,2,3,4], Ankelien S. Duchow[1,2,3], Sven Jarius[9], Jens Kuhle[10], Pascal Benkert[11], Alexander U. Brandt[1,2,3,12], Judith Bellmann-Strobl[1,2,3,4], Tanja Schmitz-Hübsch[1,2,3,4], Friedemann Paul[1,2,3,4,5], Klemens Ruprecht[#5], Hanna G. Zimmermann[#1,2,3,4,$]

1) Experimental and Clinical Research Center, a cooperation between the Max Delbrück Center for Molecular Medicine in the Helmholtz Association and the Charité – Universitätsmedizin Berlin, Berlin, Germany
2) Charité – Universitätsmedizin Berlin, corporate member of Freie Universität Berlin and Humboldt-Universität zu Berlin, Berlin, Germany
3) Max-Delbrück Center for Molecular Medicine in the Helmholtz Association, Berlin, Germany
4) NeuroCure Clinical Research Center, Charité – Universitätsmedizin Berlin, corporate member of Freie Universität Berlin and Humboldt-Universität zu Berlin, Berlin, Germany
5) Department of Neurology, Charité – Universitätsmedizin Berlin, corporate member of Freie Universität Berlin and Humboldt-Universität zu Berlin, Berlin, Germany
6) Institute for Biometry and Clinical Epidemiology, Charité – Universitätsmedizin Berlin, corporate member of Freie Universität Berlin and Humboldt-Universität zu Berlin, Germany
7) Berlin Institute of Health, Berlin, Germany
8) Department of Neurology, University of California San Francisco, CA, USA
9) Molecular Neuroimmunology Group, Department of Neurology, University of Heidelberg, Heidelberg, Germany
10) Neurology Clinic and Policlinic, MS Center and Research Center for Clinical Neuroimmunology and Neuroscience Basel (RC2NB), University Hospital Basel, Switzerland, Switzerland

11) Clinical Trial Unit, Department of Clinical Research, University Hospital Basel, University of Basel, Basel, Switzerland
12) Department of Neurology, University of California Irvine, CA, USA

* These authors contributed equally to this work, ranked by alphabetical orders.

# These authors contributed equally to this work, ranked by alphabetical orders.

$ Corresponding author

FOOTNOTE

Corresponding Author:

Hanna G. Zimmermann, Ph.D.

Experimental and Clinical Research Center, Lindenberger Weg 80, 13125 Berlin

Phone: +49 30 450 539 797

Fax: +49 450 539 915

E-mail: hanna.zimmermann@charite.de

Submission Type: Original Research Article

Title Character Count: 151

Number of Tables: 5 + 5 (supplementary)

Number of Figures: 2 + 1 (supplementary)

Word Count of Abstract: 216

Word Count of Paper: 3445

References: 36

Keywords: Neuromyelitis optica spectrum disorder, Myelin oligodendrocyte glycoprotein antibody associated disease, Optical coherence tomography, Foveal morphometry, Serum glial fibrillary acidic protein, Serum neurofilament light chain protein

Abstract

Background: Aquaporin-4 immunoglobulin-G positive (AQP4-IgG$^+$) neuromyelitis optica spectrum disorder (NMOSD) is an autoimmune astrocytopathy associated with optic neuritis (ON). Myelin oligodendrocyte glycoprotein antibody-associated disease (MOGAD) is an oligodendrocytopathy with similar phenotype. Serum glial fibrillary acidic protein (sGFAP), an astrocyte-derived protein, is associated with disease severity in AQP4-IgG$^+$ NMOSD. Serum neurofilament light (sNfL) indicates neuroaxonal damage. The objective was to investigate the association of sGFAP and sNfL with subclinical afferent visual system damage in clinically stable AQP4-IgG$^+$ NMOSD and MOGAD patients.

Methods: In this cross-sectional study, clinically stable patients with AQP4-IgG$^+$ NMOSD (N=33) and MOGAD (N=16), as diseased controls, underwent sGFAP and sNfL measurements by single molecule array, retinal optical coherence tomography and visually evoked potentials.

Results: Higher sGFAP concentrations were associated with thinner ganglion cell-inner plexiform layer (β(95% confidence interval (CI)) = -0.75(-1.23 to -0.27), p=0.007) and shallower fovea (average pit depth: β(95%CI) = -0.59(-0.63 to -0.55), p=0.020) in NMOSD non-ON eyes. Participants with pathological P100 latency had higher sGFAP (median [interquartile range]: 131.32 [81.10–179.34] vs. 89.50 [53.46–121.91]pg/ml, p=0.024). In MOGAD, sGFAP was not associated with retinal structural or visual functional measures.

Conclusions: The association of sGFAP with structural and functional markers of afferent visual system damage in absence of ON suggests that sGFAP may be a sensitive biomarker for chronic disease severity in clinically stable AQP4-IgG$^+$ NMOSD.

1. Introduction

Neuromyelitis optica spectrum disorder (NMOSD) is a disabling inflammatory disease of the CNS. In approximately 80% of patients with NMOSD, pathogenic immunoglobulin G (IgG) autoantibodies against the astrocytic water channel aquaporin-4 (AQP4) are detectable in serum.[1] AQP4-IgG positive (AQP4-IgG$^+$) NMOSD is thus considered an autoimmune astrocytopathy. A subset of patients with AQP4-IgG negative (AQP4-IgG$^-$) NMOSD exhibits IgG autoantibodies against myelin oligodendrocyte glycoprotein (MOG). MOG-antibody associated disease (MOGAD) is now recognized as a disease entity distinct from AQP4-IgG$^+$ NMOSD and an autoimmune oligodendrocytopathy.[2,3] The broadening spectrum of therapeutic options for NMOSD increases the need for disease severity and prognostic biomarkers to guide treatment decisions.[4]

Optic neuritis (ON) is a core feature of NMOSD.[5] Retinal optical coherence tomography (OCT) allows for detailed quantification of the retinal layer structures in vivo. In NMOSD, thinning of the peripapillary retinal nerve fiber layer (pRNFL) and combined macular ganglion cell and inner plexiform layer (GCIPL) indicate retinal neuroaxonal damage and correlate with functional visual parameters.[6–8] Furthermore, foveal morphological changes, such as greater pit flat disk diameter and lower inner rim volume, may identify NMOSD-specific optic neuropathy or primary retinopathy.[9] Subtle structural retinal changes, particularly foveal shape changes and GCIPL thinning, can also be detected independent of ON in NMOSD.[10,11]

Glial fibrillary acidic protein (GFAP) is an emerging biomarker in AQP4-IgG$^+$ NMOSD. As GFAP is most prominently expressed in astrocytes[12], it is hypothesized to correlate especially well with astrocytopathy, as opposed to oligodendrocyte or neuroaxonal pathology. We and others have previously shown that increased serum GFAP (sGFAP) levels are associated with disease severity, mainly assessed by EDSS, in AQP4-IgG$^+$ NMOSD[13–16], and that sGFAP concentrations in remission correlate with future attack risk.[15,16] In addition, serum neurofilament light chain (sNfL), a biomarker for neuroaxonal damage, was found to be

associated with disease severity in NMOSD.[13,15] Yet, data on the association of sGFAP and sNfL with afferent visual system damage in NMOSD are scarce.[17]

In the present study, we explored the association of sGFAP with afferent visual system damage in AQP4-IgG$^+$ NMOSD as determined by comprehensive OCT and visual function analyses. To assess specificity for astrocytopathy, we included patients with MOGAD, an oligodendrocytopathy, as controls and additionally analyzed the association of visual parameters with sNfL.

2. Materials and Methods

2.1 Study design

Thirty-three AQP4-IgG$^+$ NMOSD patients and sixteen MOGAD patients, who participate in an ongoing longitudinal observational cohort study at Charité – Universitätsmedizin Berlin, were recruited from August 2015 to March 2018 and included in this cross-sectional study. Inclusion criteria were age between 18 and 75 years, and a confirmed diagnosis of AQP4-IgG$^+$ NMOSD according to the 2015 IPND consensus criteria[5] or MOGAD according to the Jarius et al. criteria.[18] Exclusion criteria were any neurological or ophthalmological disorders unrelated to NMOSD or MOGAD affecting OCT analyses, including a refractive error above ±6 diopters. The patients analyzed in the present work were in clinical remission (last attack within 90 days in 1/33 NMOSD and 2/16 MOGAD)[15], and are identical to those studied in a previous investigation of sGFAP as disease severity and activity biomarker in NMOSD.[15] The Charité - Universitätsmedizin Berlin institutional ethics committee approved the study protocol (EA1/041/14). Written informed consent was obtained from all participants.

At study inclusion, a comprehensive medical history was obtained, and all patients underwent detailed neurological examination and ophthalmological assessments, including visually evoked potentials (VEP), visual acuity and OCT scans. Expanded Disability Status Scale (EDSS) was scored by trained raters. All individuals were tested for serum AQP4-IgG and MOG-IgG by use of fixed cell-based assay (CBA) employing full-length human AQP4 or MOG protein.[19,20] sGFAP and sNfL measurements were performed as previously described.[13,15,21]

2.2 Optical coherence tomography

We used Spectralis spectral domain OCT (Heidelberg Engineering, Heidelberg, Germany) with automatic real time (ART) averaging and active eye tracking to acquire retinal OCT images. Methodological details are described in supplementary material. All scans underwent quality control in accordance with the OSCAR-IB criteria[22] and are reported following the APOSTEL recommendations.[23] Only OCT scans that passed the quality review were included (56 eyes in the AQP4-IgG$^+$ NMOSD group and 26 eyes in the

MOGAD group). Because of profound structural changes in eyes with a history of ON (ON^+), we only included eyes without ON history (ON^-) (AQP4-IgG^+: N=34 eyes from 25 patients, MOGAD: N=11 eyes from 8 patients) in OCT analyses (Figure e-1).

2.3 Foveal morphometry parameters

After importing the OCT macular volume scans, foveal morphometry parameters were computed through our pre-established 3D foveal morphometry pipeline.[9,24] Three-dimensional macular scans are flattened based on the segmentation of the Bruch's membrane (reference plane). Three disks or planes are identified after radially reconstructing the inner limiting membrane (ILM) surface: rim disk (connection of the rim points or points with maximum height), slope disk (connection of points with maximum slopes in the parafoveal area), and pit flat disk (foveal pit plane) (Figure 1).

Eight foveal morphometry parameters were measured, including three parameters that have been previously described as specific for AQP4-IgG^+ NMOSD[9], i.e. (1) average slope disk diameter: the average of the slope disk diameters on the reconstructed radial scans, (2) average pit flat disk diameter: the average of the pit flat disk diameters on the reconstructed radial scans, and (3) inner rim volume: the volume between the reconstructed ILM surface and the reference plane within 1-mm-diameter cylinder centered at the fovea. The other five parameters included in the study were: (1) average rim disk diameter: the average of the rim disk diameters on the reconstructed radial scans, (2) rim volume: the volume between the ILM surface and the reference plane within the rim points, (3) average rim height: average height of the rim points, (4) pit depth: distance between the lowest point of the fovea and the center of rim disk, and (5) central foveal thickness: distance between the lowest point of the fovea and the reference plane.

Figure 1. Schematic illustration of foveal morphometry parameters

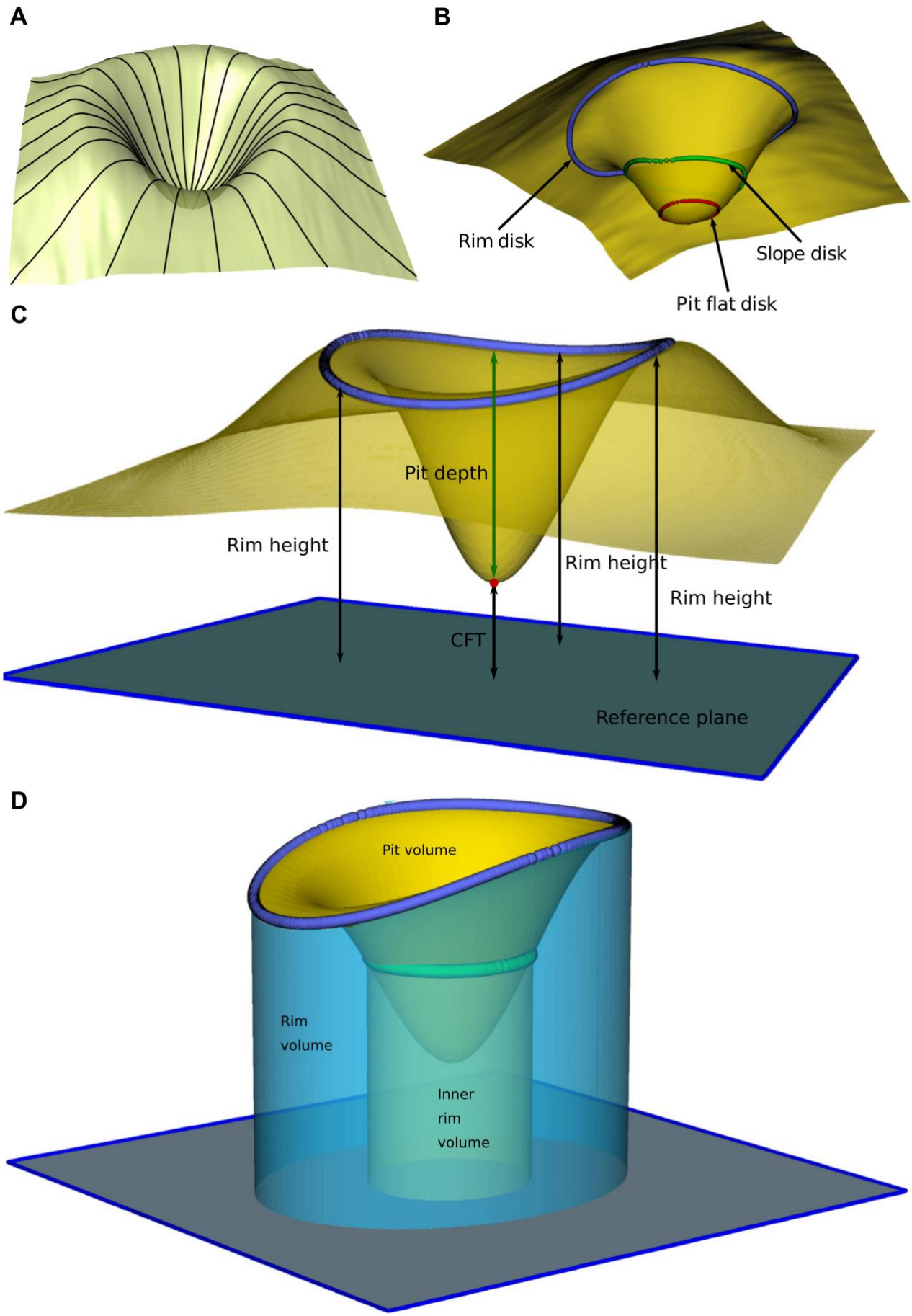
A
B
Rim disk
Slope disk
Pit flat disk
C
Pit depth
Rim height
Rim height
Rim height
CFT
Reference plane
D
Pit volume
Rim
volume
Inner
rim
volume

160

(A) Smoothed and reconstructed inner limiting membrane surface using cubic Bezier polynomial model. Foveal morphometry parameters include (B) average diameter of the three surfaces (rim disk, slope disk, pit flat disk), (C) average rim height, average foveal pit depth and central foveal thickness, and (D) rim volume and inner rim volume.

Abbreviations: CFT: central foveal thickness.

2.4 Visual function measures

VEP were recorded according to the ISCEV protocol with gold cup electrodes at Oz (active) and Fz (reference)[25] using the RETI-port/scan 21 device (Roland Consult GmbH, Brandenburg, Germany). P100 latencies were recorded. Visual acuity was tested unilaterally and followed the ETDRS protocol. High-contrast best corrected visual acuity (HCVA) was measured and reported using logarithm of the minimum angle of resolution (logMAR) charts (Precision Vision, LaSalle, Illinois, USA). Low-contrast best corrected visual acuity (LCVA) was tested with Sloan low contrast letter acuity charts at 2.5% contrast levels. Subjects with prolonged (>117ms) / extinguished P100 latency, HCVA >0.1 logMAR, LCVA >0.3 logMAR in at least one eye were classified as "abnormal VEP/HCVA/LCVA". All eyes were included in relevant analyses, regardless of the ON status.

2.5 Statistical analysis

As descriptive measures, absolute and relative frequencies, mean and standard deviation, median and interquartile ranges are reported depending on the scaling of the variables. Standardized effect size measures (standardized mean difference, SMD) were calculated to compare the characteristics differences between patients with AQP4-IgG^{+} NMOSD and patients with MOGAD, as well as to compare the differences of retinal OCT measures between eyes with and without ON history within each patient subgroups. A SMD value of >0.8, 0.5-0.8, and 0.2-0.5 represented a large, medium, and small magnitude of effect, respectively.

As the distribution of sGFAP values was positively skewed, rank-based inverse normal transformation of sGFAP values was applied before parametric analyses. Furthermore, age-adjusted Z-scores of sNfL levels (sNfLz) were calculated using Generalized Additive Models for Location Scale and Shape, as previously described.[26] The associations between sGFAP or sNfLz and retinal OCT measures were investigated using linear mixed-effect models (LMM) (dependent variables: OCT measures; independent fixed effect for sGFAP and Age or sNfLz; random intercepts for subjects). Results are reported as standardized regression coefficient (β) with 95% confidence interval (CI). Analyses of associations with visual function data were performed using group comparison with Wilcoxon rank-sum test to account for pathological VEP with unmeasurable latency due to very low amplitude, and because visual acuity measures are ordinal variables.

Interaction analyses were performed to evaluate whether the association between sGFAP or sNfL with afferent visual system damage was affected by non-ON-derived CNS damage and time since last attack. We reported the effect size of interaction using partial eta squared (η_p^2).

Statistical analysis was performed in R version 4.0.2 with tableone, lme4, lmerTest, MuMIn, ggplot2, ggpubr, and effectsize packages. A two-sided significance level of α=0.05 was used. Due to the exploratory nature of this study, no correction for multiple testing was performed. Interpretation of p-values should be done cautiously. Interpretation of results is mainly based on effect sizes and 95%CI.

205 # 3. Results

206 ## 3.1 Characteristics of the study population

207 Forty-nine participants (33 with AQP4-IgG$^+$ NMOSD and 16 with MOGAD) were included. Demographic
208 data and clinical characteristics were as previously reported[15], and are summarized in Table 1. Further
209 clinical characteristics and their associations with sGFAP and sNfL were reported in our previous study[15].
210 Compared with MOGAD, more female patients, a longer time since last relapse and a higher median EDSS
211 score were observed in AQP4-IgG$^+$ NMOSD. Both sGFAP levels and sNfLz levels did not substantially
212 differ between the two groups. The observed retinal structural and visual functional changes in eyes with
213 prior ON were in line with previous reports (Table 2).[6–9] No relevant differences were observed between
214 the AQP4-IgG$^+$ and MOG-IgG$^+$ groups in any structural or functional visual parameters (Table 2).

215

216 **Table 1.** Patient characteristics by serostatus

	AQP4-IgG$^+$ (N = 33)	**MOG-IgG$^+$ (N = 16)**	**SMD**
Sex (F (%) / M (%))	30 (90.9%) / 3 (9.1%)	10 (62.5%) / 6 (37.5%)	0.71
Age (years) Mean (SD)	49.6 (13.6)	46.0 (15.4)	0.25
Disease duration (months) Median [IQR]	79 [52 – 108]	50 [10 – 148]	0.04
Time since last attack (months) Median [IQR]	26 [11 – 56]	8 [4 – 24]	0.52
Last attack type (N (%))			0.61
	ON: 12 (36.4%)	ON: 10 (62.5%)	
	Myelitis: 19 (57.6%)	Myelitis: 6 (37.5%)	
	Others: 2 (6.1%)	Others: 0 (0.0%)	
Number of eyes (N)	56	26	-
Eyes with a history of ON (N (%)) - of which single ON episode	22 (39.3%) 10 (45.5%)	15 (57.7%) 3 (20.0%)	0.44

ON episodes per eye (N) Median [Range]	2 [1 – 8]	2 [1 – 8]	-
Patients with history of myelitis (N (%))	27 (81.8%)	9 (56.3%)	0.58
Myelitis episodes per patients (N) Median [Range]	1 [0 – 10]	1 [0 – 5]	-
Immunotherapy	RTX: 20 (60.6%)	RTX: 8 (50.0%)	-
	AZA: 6 (18.2%)	AZA: 1 (6.3%)	
	MMF: 1 (3.0%)	MMF: 1 (6.3%)	
	BEL: 1 (3.0%)	GLC: 2 (12.5%)	
	TCZ: 1 (3.0%)		
	No Treatment: 4 (12.1%)	No Treatment: 4 (25.0%)	
sGFAP level (pg/ml) Median [IQR]	109.2 [63.1 – 154.8]	81.1 [58.2 – 116.9]	0.03
sNfL level (pg/ml) Median [IQR]	21.9 [16.6 – 41.4]	26.6 [15.9 – 43.7]	0.23
EDSS score Median [IQR]	4.0 [2.0 – 5.0]	2.5 [2.0 – 3.0]	0.63
MSFC Mean (SD)	-0.03 (0.69)	0.25 (0.58)	0.44

Abbreviations: AQP4-IgG: aquaporin-4 immunoglobulin G; AZA: azathioprine; BEL: belimumab; EDSS: Expanded Disability Status Scale; GLC: glucocorticoids; IQR: interquartile range; MMF: mycophenolate mofetil; MOG-IgG: myelin oligodendrocyte protein immunoglobulin G; MSFC: multiple sclerosis functional composite; N = number of patients; ON: optic neuritis; SD: standard deviation; sGFAP: serum glial fibrillary acidic protein; SMD: standardized mean difference; sNfL: serum neurofilament light chain; RTX: rituximab; TCZ: tocilizumab.

Table 2. OCT and foveal morphometry results by serostatus and ON history

	AQP4-IgG$^+$			**MOG-IgG$^+$**		
	ON$^-$ (N = 34)	**ON$^+$ (N = 22)**	**SMD**	**ON$^-$ (N = 11)**	**ON$^+$ (N = 15)**	**SMD**

pRNFL thickness (μm) Mean (SD)	91.79 (15.46)	60.69 (22.75)	1.60	93.64 (18.63)	52.95 (17.25)	2.27
mRNFL thickness (μm) Mean (SD)	35.16 (3.64)	26.95 (6.75)	1.51	35.37 (4.18)	23.53 (4.03)	2.88
GCIPL thickness (μm) Mean (SD)	73.60 (8.14)	56.59 (11.50)	1.71	75.97 (8.30)	52.23 (9.29)	2.70
INL thickness (μm) Mean (SD)	37.58 (3.28)	40.51 (4.48)	0.75	39.67 (2.05)	41.66 (3.85)	0.65
OPL thickness (μm) Mean (SD)	25.39 (2.31)	25.42 (1.19)	0.02	24.72 (1.53)	24.78 (1.46)	0.04
ONL thickness (μm) Mean (SD)	61.18 (5.86)	67.93 (8.44)	0.93	62.94 (4.54)	65.10 (5.39)	0.43
Central foveal thickness (μm) Mean (SD)	270.68 (16.32)	269.04 (20.70)	0.09	278.82 (19.16)	269.93 (12.49)	0.55
Average rim disk diameter (mm) Mean (SD)	2.14 (0.14)	2.07 (0.12)	0.56	2.16 (0.14)	2.02 (0.08)	1.38
Average slope disk diameter (mm) Mean (SD)	0.75 (0.14)	0.73 (0.15)	0.15	0.66 (0.16)	0.63 (0.11)	0.19
Average pit flat disk diameter (mm) Mean (SD)	0.24 (0.04)	0.26 (0.07)	0.25	0.21 (0.04)	0.22 (0.02)	0.22
Inner rim volume (mm^3) Mean (SD)	0.09 (0.02)	0.09 (0.02)	0.01	0.11 (0.02)	0.10 (0.01)	0.44
Rim volume (mm^3) Mean (SD)	0.96 (0.18)	0.84 (0.19)	0.61	1.04 (0.18)	0.79 (0.10)	1.66
Average pit depth (mm) Mean (SD)	0.11 (0.03)	0.09 (0.03)	0.61	0.12 (0.02)	0.09 (0.02)	1.57
Average rim height (mm) Mean (SD)	0.34 (0.02)	0.32 (0.03)	0.83	0.35 (0.02)	0.32 (0.02)	1.96
P100 Latency (ms)	117.42 (18.62)	130.64 (22.96)	0.63	111.42 (6.64)	136.74 (20.75)	1.64

Mean (SD)						
LogMAR HCVA Median [IQR]	-0.1 [-0.2 – 0.0]	0.0 [0.0 – 0.2]	0.75	-0.05 [-0.2 – 0.0]	-0.1 [-0.2 – 0.1]	0.15
LogMAR LCVA Median [IQR]	0.3 [0.3 – 0.5]	0.5 [0.3 – 0.6]	0.72	0.4 [0.15 – 0.4]	0.3 [0.3 – 0.6]	0.44

Abbreviations: AQP4-IgG: aquaporin-4 immunoglobulin G; GCIPL: combined macular ganglion cell and inner plexiform layer; HCVA: high-contrast visual acuity; INL: inner nuclear layer; IQR: interquartile range; LCVA: low-contrast visual acuity; logMAR: logarithm of the minimum angle of resolution; MOG-IgG: myelin oligodendrocyte protein immunoglobulin G; mRNFL: macular retinal nerve fiber layer; N = number of eyes; OCT: optical coherence tomography; ON: optic neuritis; ONL: outer nuclear layer; OPL: outer plexiform layer; pRNFL: peri-papillary retinal nerve fiber layer; SD: standard deviation; SMD: standardized mean difference.

3.2 Associations of sGFAP and sNfL with retinal layer thickness in non-ON eyes

In ON^- eyes of AQP4-IgG^+ NMOSD, higher sGFAP levels were associated with measures of retinal neuroaxonal loss, including thinner GCIPL (β(95%CI)=-0.75(-1.23 to -0.27), p=0.007; Figure 2C), thinner mRNFL (β(95%CI)=-0.91(-1.31 to -0.51), p<0.001; Figure 2B), and, to a lesser extent, thinner pRNFL (β(95%CI)=-0.44(-0.89 to 0.01), p=0.065; Figure 2A). Patients with higher sNfLz had a lower GCIPL thickness (β(95%CI)=-0.48(-0.91 to -0.05), p=0.039; Figure 2F). However, associations of sNfLz with both pRNFL (β(95%CI)=-0.31(-0.67 to 0.04), p=0.095) and mRNFL (β(95%CI)=-0.45(-0.90 to 0.00), p=0.060) thickness were less pronounced (Figure 2D–E). In MOGAD, neither sGFAP nor sNfLz were substantially associated with any of the retinal thickness measures (Figure 2G–L).

Figure 2. Association of sGFAP and sNfL with OCT parameters in ON^- eyes of AQP4-IgG^+ NMOSD and MOGAD subjects

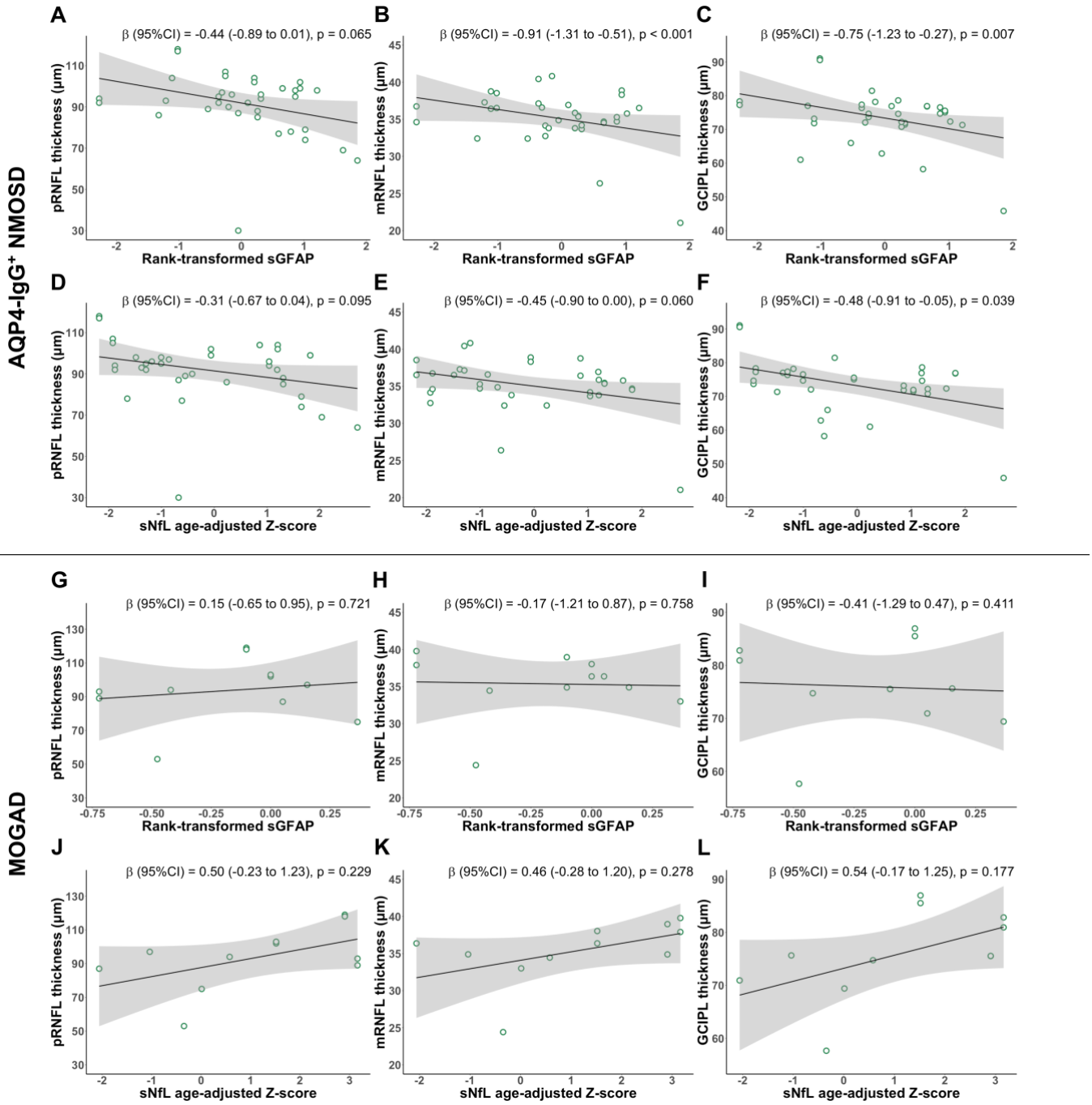

Scatterplots showing correlation between sGFAP and sNfL with pRNFL, mRNFL and GCIPL. Association of normalized rank-transformed sGFAP with (A) pRNFL thickness, (B) mRNFL thickness, (C) GCIPL thickness in AQP4-IgG$^+$ NMOSD; sNfL age-adjusted Z-score with (D) pRNFL thickness, (E) mRNFL thickness, (F) GCIPL thickness in AQP4-IgG$^+$ NMOSD; normalized rank-transformed sGFAP with (G) pRNFL thickness, (H) mRNFL thickness, (I) GCIPL thickness in MOGAD; sNfL age-adjusted Z-score with (J) pRNFL thickness, (K) mRNFL thickness, (L) GCIPL thickness in MOGAD.

Analyzed with linear mixed effect model (dependent variables: OCT measures; independent fixed effect for normalized rank-transformed sGFAP and age or sNfL age-adjusted Z-score; random intercepts for subjects) in 34 non-ON eyes from 25 AQP4-IgG$^+$ NMOSD or 11 non-ON eyes from 8 MOGAD patients. Shaded regions indicate 95% CIs.

Abbreviations: AQP4-IgG: aquaporin-4 immunoglobulin G; β: standardized estimate; CI: confidence interval; GCIPL: combined macular ganglion cell and inner plexiform layer; m: macular; MOGAD: myelin oligodendrocyte glycoprotein antibody associated disorders; NMOSD: Neuromyelitis optica spectrum disorder; OCT: optical coherence tomography; ON: optic neuritis; p: peri-papillary; RNFL: retinal nerve fiber layer; sGFAP: serum glial fibrillary acidic protein; sNfL: serum neurofilament light chain.

3.3 Associations of sGFAP and sNfL with foveal morphometry measures in non-ON eyes

In AQP4-IgG$^+$ NMOSD, higher sGFAP was associated with lower average rim disk diameter, rim volume, average pit depth and average rim height, but not with average slope disk diameter, pit flat disk diameter, inner rim volume and central foveal thickness (Table 3) of ON$^-$ eyes. Similarly, higher sNfLz correlated with lower average pit depth, average rim height and rim volume (Table 3). In MOGAD, higher sGFAP was only associated with lower average rim height (Table e-1). sNfLz was slightly lower in patients with MOGAD with lower average rim height (Table e-1).

Table 3. Association of sGFAP and sNfL with foveal morphometry parameters in AQP4-IgG$^+$ NMOSD subjects

	Normalized rank-transformed sGFAP		**sNfL age-adjusted Z-score**	
	β (95%CI)	***p*-value**	**β (95%CI)**	***p*-value**
Average rim disk diameter (mm)	-0.55 (-0.96 to -0.14)	0.019	-0.40 (-0.77 to -0.02)	0.052
Average slope disk diameter (mm)	-0.19 (-0.70 to 0.32)	0.469	0.18 (-0.23 to 0.59)	0.402
Average pit flat disk diameter (mm)	0.05 (-0.50 to	0.874	0.21 (-0.24 to 0.66)	0.368

	0.60)			
Inner rim volume (mm^3)	0.02 (-0.51 to 0.55)	0.932	-0.26 (-0.69 to 0.17)	0.234
Rim volume (mm^3)	-0.60 (-1.01 to -0.19)	0.011	-0.52 (-0.87 to -0.17)	0.010
Average pit depth (mm)	-0.59 (-0.63 to -0.55)	0.020	-0.45 (-0.84 to -0.06)	0.034
Average rim height (mm)	-0.79 (-1.24 to -0.34)	0.003	-0.63 (-1.02 to -0.24)	0.004
Central foveal thickness (mm)	0.11 (-0.42 to 0.64)	0.690	-0.05 (-0.50 to 0.40)	0.838

Analyzed with separate linear mixed effect models (dependent variables: OCT measures; independent fixed effect for normalized rank-transformed sGFAP and age or sNfL age-adjusted Z-score; random intercepts for subjects) in 34 non-ON eyes from 25 AQP4-IgG^+ NMOSD patients.

Abbreviations: AQP4-IgG: aquaporin-4 immunoglobulin G; β: standardized estimate; CI: confidence interval; ON: optic neuritis; sGFAP: serum glial fibrillary acidic protein; sNfL: serum neurofilament light chain.

3.4 Relation of sGFAP and sNfL with visual function and electrophysiological measures

In the AQP4-IgG^+ NMOSD group, participants with abnormal VEP P100 latency showed modestly higher sGFAP concentrations than those with normal VEP latency (median [IQR]: 131.32pg/ml [81.10–179.34] vs. 89.50pg/ml [53.46–121.91], p=0.024). Additionally, higher sGFAP levels were also detected in patients with abnormal LCVA compared to subjects with normal LCVA (median [IQR]: 128.98pg/ml [95.90–161.23] vs. 81.10pg/ml [51.17–100.18], p=0.011). A similar, yet less pronounced difference was found between patients with abnormal and normal HCVA (median [IQR]: 149.21pg/ml [80.49–225.49] vs. 101.85pg/ml [73.43–131.32], p=0.123). The differences in sNfLz between patients with abnormal and normal VEP latency, HCVA and LCVA were even less pronounced (Table 4). No relevant difference in

sGFAP or sNfL concentrations according to VEP latency, HCVA or LCVA was detected in participants with MOGAD (Table e-2).

Table 4. sGFAP and sNfL concentrations in AQP4-IgG$^+$ NMOSD subjects with normal and abnormal visual function

	P100 Latency			LogMAR HCVA			LogMAR LCVA		
	Normal	**Abnormal**	***p*-value**	**Normal**	**Abnormal**	***p*-value**	**Normal**	**Abnormal**	***p*-value**
sGFAP (pg/ml) Median [IQR]	89.50 [53.46 – 121.91]	131.32 [81.10 – 179.34]	0.024	101.85 [73.43 – 131.32]	149.21 [80.49 – 225.49]	0.123	81.10 [51.17 – 100.18]	128.98 [95.90 – 161.23]	0.011
sNfL age-adjusted Z-score Median [IQR]	-0.78 [-1.45 – 0.91]	-0.06 [-0.92 – 1.31]	0.116	-0.86 [-1.29 – 0.86]	0.24 [-0.61 – 1.73]	0.096	-0.68 [-1.19 – 0.53]	-0.42 [-1.24 – 1.25]	0.445

Group comparison analyzed with Wilcoxon rank-sum test in all 33 AQP4-IgG$^+$ NMOSD patients.

Abbreviations: AQP4-IgG: aquaporin-4 immunoglobulin G; HCVA: high-contrast visual acuity; IQR: interquartile range; LCVA: low-contrast visual acuity; logMAR: logarithm of the minimum angle of resolution; sGFAP: serum glial fibrillary acidic protein; sNfL: serum neurofilament light chain.

3.5 Subgroup analyses

To account for non-ON-derived CNS injury as a possible confounder for the associations between sGFAP and sNfL and parameters of afferent visual system damage, we conducted subgroup analyses in AQP4-IgG$^+$ NMOSD patients with unimpaired and impaired walking ability as indicated by an EDSS score ≤3 (n=17) or >3 (n=17). Interaction analyses showed no relevant inter-group difference between patients with EDSS scores ≤ 3 and > 3 with respect to the associations of either sGFAP (Table 5) or sNfL (Table e-4) with GCIPL, mRNFL and pRNFL in ON$^-$ eyes. The associations of sGFAP (Table e-3) or sNfLz (Table e-4) with foveal morphometry parameters also did not differ between the two groups. Due to low sample size, we refrained from subgroup analyses within the MOGAD group, and regarding VEP latencies and visual acuity (group comparisons within subgroups).

Furthermore, we investigated subgroups of AQP4-IgG$^+$ NMOSD patients with (myelitis, n=10; area postrema syndrome, n=2) or without (n=22) a non-ON attack within one year prior to study inclusion. Interaction analyses revealed inter-group differences for GCIPL (η_p^2=0.29, p=0.036) and mRNFL (η_p^2=0.26, p=0.039), both of which were more strongly associated with sGFAP in subjects with an attack in the last year (Table 5). Associations of sNfL with inner retinal layer thickness, particularly GCIPL and mRNFL, were numerically more profound in patients with an attack within the last year (Table e-4).

Lastly, to evaluate whether sGFAP and sNfL can also be considered as biomarkers for attack-dependent structural afferent visual system damage, the associations of both biomarkers with retinal OCT measures in ON$^+$ eyes of AQP4-IgG$^+$ NMOSD patients (22 eyes in 19 patients) were additionally analyzed. As opposed to the findings in ON$^-$ eyes, no correlation of higher sGFAP or sNfL with thinner GCIPL, pRNFL, or mRNFL was observed (Table e-5). Furthermore, we observed group differences between ON$^+$ and ON$^-$ eyes regarding the association of sGFAP with GCIPL (η_ρ^2=0.11, p=0.032), and to a lesser degree, with pRNFL (η_ρ^2=0.06, p=0.071) and mRNFL (η_ρ^2=0.07, p=0.060). None of the foveal morphometry parameters was associated with sGFAP or sNfL in ON$^+$ eyes (Table e-5).

Table 5. Association of sGFAP with retinal layer thickness in subgroups of AQP4-IgG$^+$ NMOSD subjects with EDSS ≤ 3 or > 3 and last attack within ≤ 1 year or > 1 year

		EDSS		**Time since last non-ON attack**	
		≤ 3.0 (N = 17)	> 3.0 (N = 17)	≤ 1 Year (N = 12)	> 1 Year (N = 22)
pRNFL thickness (µm)	β (95%CI)	-0.44 (-1.20 to 0.32)	-0.23 (-0.76 to 0.30)	-0.40 (-1.09 to 0.29)	-0.58 (-1.29 to 0.13)
	p-value	0.291	0.410	0.297	0.136
	η_ρ^2 for interaction with sGFAP, *p*-value	$\eta_\rho^2 = 3.83e^{-4}$, $p = 0.923$		$\eta_\rho^2 = 0.04$, $p = 0.360$	

mRNFL thickness (μm)	β (95%CI)	-0.72 (-1.33 to -0.11)	-0.76 (-1.15 to -0.37)	-0.94 (-1.47 to -0.41)	-0.74 (-1.35 to -0.13)
	p-value	0.050	0.004	0.017	0.036
	η_p^2 for interaction with sGFAP, *p*-value	$\eta_p^2 = 0.06$, $p = 0.290$		$\eta_p^2 = 0.21$, $p = 0.038$	
GCIPL thickness (μm)	β (95%CI)	-0.46 (-1.24 to 0.32)	-0.62 (-1.11 to -0.13)	-0.77 (-1.40 to -0.14)	-0.62 (-1.44 to 0.20)
	p-value	0.288	0.036	0.062	0.172
	η_p^2 for interaction with sGFAP, *p*-value	$\eta_p^2 = 0.02$, $p = 0.539$		$\eta_p^2 = 0.22$, $p = 0.037$	

Analyzed with linear mixed effect model (dependent variables: OCT measures; independent fixed effect for normalized rank-transformed sGFAP and age; random intercepts for subjects) in 34 non-ON eyes from 25 AQP4-IgG$^+$ NMOSD patients. An interaction term of normalized rank-transformed sGFAP and each sub-group was included to assess the inter-group differences.

Abbreviations: AQP4-IgG: aquaporin-4 immunoglobulin G; β: standardized estimate; CI: confidence interval; η_p^2: partial eta-squared; EDSS: Expanded Disability Status Scale; GCIPL: combined macular ganglion cell and inner plexiform layer; mRNFL: macular retinal nerve fiber layer; N: number of eyes; ON: optic neuritis; pRNFL: peri-papillary retinal nerve fiber layer; sGFAP: serum glial fibrillary acidic protein.

4. Discussion

This detailed cross-sectional study investigating patients with clinically stable AQP4-IgG$^+$ NMOSD showed that elevated sGFAP concentrations are associated with retinal neuroaxonal loss, as evidenced by thinner GCIPL as well as mRNFL and pRNFL, and with foveal flattening, as assessed by foveal morphometry in ON$^-$ eyes. On a functional level, patients with pathologic VEP P100 latencies and LCVA exhibited higher sGFAP levels. sNfL was associated with structural measures (GCIPL, foveal morphometry parameters) in ON$^-$ eyes, but not with functional (VEP, HCVA, LCVA) measures of afferent visual system damage. In a control group of MOGAD patients, no analogous associations with either serum biomarker were detected.

The consistent association of increased sGFAP concentrations with retinal neuroaxonal loss and impaired afferent visual system function indicates that sGFAP may be a sensitive biomarker for visual system damage in AQP4-IgG$^+$ NMOSD, extending the previously demonstrated correlation of sGFAP with disability.[13,15,16] Yet, in contrast to a recent study by Aly and colleagues[17], we did not observe higher sGFAP levels in patients with lower foveal thickness. The comparability of both studies is, however, limited due to the inclusion of six AQP4-IgG$^-$ patients (of a total of 16) and patients with ON$^+$ eyes in the study by Aly and colleagues.[17]

Both subclinical ON and subclinical primary retinopathy have been hypothesized to underlie attack-unrelated visual system damage.[9,27] In NMOSD, ON-independent changes result in a widened, “U-shaped” fovea[9,27], whereas ON leads to a shallower, “V-shaped” fovea, next to thinning of RNFL and GCIPL, indicating neuroaxonal damage.[9,27] Unexpectedly, we observed an association of sGFAP in ON$^-$ eyes not only with RNFL and GCIPL thinning, but also with an “ON-type” fovea. Taken together, this suggests that sGFAP is a highly sensitive biomarker for subclinical neuroaxonal optic nerve damage, rather than for the previously proposed primary retinopathy in AQP4-IgG$^+$ NMOSD.

Less pronounced and less consistent associations of sNfL with OCT and foveal morphometry measures of visual system damage as well as lack of association with functional visual assessments point at a limited value of sNfL as a biomarker for visual system affection in AQP4-IgG$^+$ NMOSD, as compared to sGFAP. This corresponds to relatively weaker associations of sNfL with disability and future disease activity in AQP4-IgG$^+$ NMOSD[14,15] and is in accordance with the pathophysiological concept of AQP4-IgG$^+$ NMOSD being primarily an astrocytopathy. Nonetheless, these results corroborate the value of sNfL as a sensitive general marker for neuroaxonal damage.

The absent associations in the control cohort of patients with MOGAD indicate specificity of sGFAP as a biomarker for afferent visual system damage in AQP4-IgG$^+$ NMOSD. This supports the concept, that sGFAP concentrations reflect astrocyte rather than oligodendrocyte dominated pathology. Two limitations of this conclusion must be regarded. First, unequal group size in the MOGAD group may cause a relatively higher chance for a type II error. Yet, effect sizes, which are independent of sample size, were consistently lower in MOGAD. Second, not only sGFAP, but also sNfL lacked associations with visual parameters in MOGAD. This could imply that these missing effects were no result of sGFAP's specificity for astrocytopathy. However, our patients were in stable remission, hence subclinical disease activity may be the basis of our findings. While there is growing evidence for subclinical disease activity in AQP4-IgG$^+$ NMOSD, there is considerable uncertainty in MOGAD.[28] Less attack-independent disease activity in MOGAD could explain missing associations of both sGFAP and sNfL with visual parameters.

GFAP levels in CSF are higher in patients with spinal cord lesions and depend on lesion length[29], indicating that sGFAP levels are dependent on the mass of affected CNS tissue. Therefore, it could be argued that the extent of tissue damage in ON could be too low to cause any measurable sGFAP increase. Additionally, even a detectable ON-derived sGFAP increase might be blurred by elsewhere located CNS-inflammation. However, the stronger associations between sGFAP and GCIPL as well as mRNFL in patients with a non-ON-attack within one year argues against a relevant confounding effect of attack-derived CNS-tissue

damage. Likewise, the independency of associations between sGFAP and OCT parameters from walking ability suggests that the value of sGFAP as a marker for visual system involvement might persist independent of chronic CNS lesions.

Despite the consistent association of sGFAP with measures of afferent visual system affection, it is not certain that this is indeed the source of GFAP. Given the low tissue mass of optic nerve and retina, an increase of sGFAP might reflect general subclinical astrocytopathy. The pronounced association of sGFAP with GCIPL and RNFL in patients with a recent attack in ON^- eyes and irrespective of lesion site might support this notion. However, sGFAP levels in NMOSD patients in stable remission are not associated with time since the last attack.[15] Nonetheless, the precise site from which elevated sGFAP in patients with NMOSD originates currently remains unclear. Therefore, further investigations on experimental models are needed to clarify this point.

Several lines of evidence suggest subclinical inter-attack disease activity in AQP4-IgG^+ NMOSD.[30] Our findings could be considered to imply subclinical ON. However, there are several restraints on these interpretations. First, ON-independent foveal alterations have been attributed to retinal astrocytopathy in the form of Müller cell injury rather than to subclinical ON.[9,27] However, signs of neuroaxonal damage have also been reported in ON^- eyes.[9,11,27,31,32] One possible explanation for the association of sGFAP with OCT-indicators of neuroaxonal damage but not primary retinopathy may be the overall low volume of retinal tissue. Furthermore, GFAP expression in Müller cells is strongly increased only under severe stress[33,34] and might therefore be low outside clinically overt attacks. Second, our results could be due to secondary neurodegeneration instead of inter-attack disease activity. While the absence of associations between sGFAP and measures of afferent visual system damage in eyes with a history of overt ON generally supports the notion of attack-independent disease activity, it does not preclude secondary contralateral neurodegeneration. This is an important aspect, as we included contralateral ON^- eyes of patients with a history of ON. ON in NMOSD often affects the optic chiasm and consecutive bidirectional

neurodegeneration has been reported.[32] Since MRI-based assessments of optic chiasm involvement were not available from the patients included in this work, this possibility cannot be excluded.[35] However, one would not expect secondary neurodegeneration to be specific for AQP4-IgG mediated damage. With respect to this, the absence of analogous findings in our specificity control group of MOGAD patients is an indirect argument for AQP4-IgG-specific inter-attack disease activity.

Strengths of this study include the detailed, multimodal assessments of afferent visual system function and structure in a homogenous, well-characterized study population of patients with AQP4-IgG$^+$ NMOSD and the inclusion of equally well-characterized patients with MOGAD as a rigorous specificity control.

Among the limitations of this monocentric study is the relatively low number of patients, due to the low prevalence of the two conditions. Consequently, to retain a sufficient sample size for meaningful statistics, we were not able to exclude ON$^-$ eyes of patients with a history of contralateral ON. As discussed above, cross-over effects of chiasm-involving ON can therefore not be excluded.

Altogether, this study shows that sGFAP is associated with structural and functional afferent visual system damage in patients with clinically stable AQP4-IgG$^+$ NMOSD. These findings suggest that sGFAP may be sensitive marker for disease severity in AQP4-IgG$^+$ NMOSD and add to the growing evidence for subclinical disease activity in NMOSD. However, validation in independent, larger patient populations, ideally including MRI assessment of the visual pathway as well as further preclinical research, is needed to corroborate our results. Despite the emerging role of sGFAP as biomarker in NMOSD[36], its potential value in the care of individual patients currently remains elusive.

Supplementary materials

Optical coherence tomography scanning protocol

The GCIPL thickness values were calculated as a 5-mm diameter annulus sparing the fovea from a macular volume scan (25°x30°, 61 vertical B-scans, ART=15) and the pRNFL thickness was measured through a peri-papillary scan (3.5mm diameter) (768A-scans, ART=25) around the optic nerve head. The segmentation of pRNFL and all intra-retinal layers in the macular scans was performed using SAMIRIX pipeline, as described in detail elsewhere. All scans were manually reviewed to confirm the accuracy of the segmentation.

Table e-1. Association of sGFAP and sNfL with foveal morphometry parameters in MOGAD subjects

	Normalized rank-transformed sGFAP		**sNfL age-adjusted Z-score**	
	β (95%CI)	***p*-value**	**β (95%CI)**	***p*-value**
Average rim disk diameter (mm)	-0.48 (-1.36 to 0.40)	0.329	0.40 (-0.34 to 1.14)	0.333
Average slope disk diameter (mm)	0.36 (-0.42 to 1.14)	0.408	-0.33 (-1.04 to 0.38)	0.392
Average pit flat disk diameter (mm)	0.35 (-0.55 to 1.25)	0.475	-0.13 (-0.95 to 0.69)	0.774
Inner rim volume (mm^3)	-0.59 (-1.32 to 0.14)	0.171	0.56 (-0.01 to 1.13)	0.106
Rim volume (mm^3)	-0.76 (-1.54 to 0.02)	0.113	0.65 (0.02 to 1.28)	0.087
Average pit depth (mm)	-0.55 (-1.51 to 0.41)	0.312	0.42 (-0.34 to 1.18)	0.321
Average rim height (mm)	-1.03 (-1.40 to -0.66)	0.003	0.81 (0.28 to 1.34)	0.024
Central foveal thickness (mm)	-0.64 (-146 to 0.18)	0.185	0.58 (-0.02 to 1.17)	0.106

Analyzed with separate linear mixed effect models (dependent variables: OCT measures; independent fixed effect for normalized rank-transformed sGFAP and age or sNfL age-adjusted Z-score; random intercepts for subjects) in 11 non-ON eyes from 8 MOGAD patients.

Abbreviations: β: standardized estimate; CI: confidence interval; MOGAD: myelin oligodendrocyte glycoprotein antibody associated disorders; sGFAP: serum glial fibrillary acidic protein; sNfL: serum neurofilament light chain.

Table e-2. Group comparison of sGFAP and sNfL between normal and abnormal visual function group in MOGAD subjects

	P100 Latency			LogMAR HCVA			LogMAR LCVA		
	Normal	**Abnormal**	***p*-value**	**Normal**	**Abnormal**	***p*-value**	**Normal**	**Abnormal**	***p*-value**
sGFAP (pg/ml) Median [IQR]	92.19 [76.13 – 94.10]	64.41 [56.39 – 172.60]	0.754	82.27 [56.82 – 108.78]	80.73 [69.64 – 148.27]	0.770	75.69 [56.82 – 101.01]	93.37 [71.18 – 189.81]	0.504
sNfL age-adjusted Z-score Median [IQR]	0.12 [-0.86 – 1.28]	0.34 [-0.55 – 1.16]	0.479	0.29 [-0.70 – 0.87]	0.72 [-0.64 – 2.07]	0.599	-1.02 [-2.07 – 0.80]	0.68 [-0.45 – 1.52]	0.414

Group comparison analyzed with Wilcoxon rank-sum test in all 16 MOGAD patients.

Abbreviations: HCVA: high-contrast visual acuity; IQR: interquartile range; LCVA: low-contrast visual acuity; logMAR: logarithm of the minimum angle of resolution; MOGAD: myelin oligodendrocyte glycoprotein antibody associated disorders; sGFAP: serum glial fibrillary acidic protein; sNfL: serum neurofilament light chain.

Table e-3. Association of sGFAP with foveal morphometry parameters in subgroups of AQP4-IgG$^+$ NMOSD subjects with EDSS ≤ 3 or > 3 and last attack within ≤ 1 year or > 1 year

		EDSS		**Time since last non-ON attack**	
		≤ 3.0 (N = 17)	> 3.0 (N = 17)	≤ 1 Year (N = 12)	> 1 Year (N = 22)
Average rim disk diameter (mm)	β (95%CI)	-0.50 (-1.23 to 0.23)	-0.28 (-0.85 to 0.29)	-0.44 (-1.13 to 0.25)	0.58 (-0.11 to 1.27)
	p-value	0.215	0.358	0.264	0.094
	η_p^2 for interaction with sGFAP, *p*-value	$\eta_p^2 = 7.89e^{-3}$, $p = 0.700$		$\eta_p^2 = 2.86e^{-5}$, $p = 0.982$	
Average slope disk diameter (mm)	β (95%CI)	-0.21 (-0.95 to 0.53)	0.09 (-0.48 to 0.66)	-0.22 (-1.00 to 0.56)	-0.18 (-0.96 to 0.60)
	p-value	0.603	0.772	0.610	0.666
	η_p^2 for interaction with sGFAP, *p*-value	$\eta_p^2 = 5.65e^{-3}$, $p = 0.744$		$\eta_p^2 = 5.86e^{-3}$, $p = 0.741$	

Average pit flat disk diameter (mm)	β (95%CI)	-0.23 (-0.97 to 0.51)	0.08 (-0.53 to 0.69)	0.04 (-0.82 to 0.90)	-0.16 (-0.92 to 0.60)
	p-value	0.565	0.811	0.925	0.685
	η_p^2 for interaction with sGFAP, *p*-value	$\eta_p^2 = 8.17e^{-5}$, $p = 0.969$		$\eta_p^2 = 1.68e^{-3}$, $p = 0.860$	
Inner rim volume (mm^3)	β (95%CI)	0.12 (-0.66 to 0.90)	-0.29 (-0.88 to 0.30)	-0.06 (-0.88 to 0.76)	0.09 (-0.71 to 0.89)
	p-value	0.769	0.347	0.882	0.831
	η_p^2 for interaction with sGFAP, *p*-value	$\eta_p^2 = 0.02$, $p = 0.528$		$\eta_p^2 = 1.50e^{-3}$, $p = 0.868$	
Rim volume (mm^3)	β (95%CI)	-0.48 (-1.21 to 0.25)	-0.44 (-1.01 to 0.13)	-0.5 (-1.17 to 0.17)	-0.61 (-1.24 to 0.02)
	p-value	0.227	0.158	0.203	0.079
	η_p^2 for interaction with sGFAP, *p*-value	$\eta_p^2 = 1.69e^{-3}$, $p = 0.859$		$\eta_p^2 = 5.39e^{-3}$, $p = 0.752$	
Average pit depth (mm)	β (95%CI)	-0.49 (-1.18 to 0.20)	-0.26 (-0.89 to 0.37)	-0.43 (-1.21 to 0.35)	-0.56 (-1.15 to 0.03)
	p-value	0.195	0.437	0.331	0.085
	η_p^2 for interaction with sGFAP, *p*-value	$\eta_p^2 = 4.67e^{-3}$, $p = 0.768$		$\eta_p^2 = 7.53e^{-3}$, $p = 0.709$	
Average rim height (mm)	β (95%CI)	-0.50 (-1.30 to 0.30)	-0.72 (-1.15 to -0.29)	-0.81 (-1.40 to -0.22)	-0.66 (-1.42 to 0.10)
	p-value	0.252	0.008	0.042	0.116
	η_p^2 for interaction with sGFAP, *p*-value	$\eta_p^2 = 4.39e^{-3}$, $p = 0.776$		$\eta_p^2 = 0.11$, $p = 0.152$	
Central foveal thickness (mm)	β (95%CI)	0.13 (-0.68 to 0.94)	-0.38 (-0.94 to 0.17)	-0.15 (-1.06 to 0.76)	0.15 (-0.58 to 0.88)
	p-value	0.760	0.209	0.762	0.696
	η_p^2 for interaction with sGFAP, *p*-value	$\eta_p^2 = 0.04$, $p = 0.374$		$\eta_p^2 = 0.03$, $p = 0.462$	

462 Analyzed with linear mixed effect model (dependent variables: OCT measures; independent fixed effect

for normalized rank-transformed sGFAP and age; random intercepts for subjects) in 34 non-ON eyes from 25 AQP4-IgG$^+$ NMOSD patients. An interaction term of normalized rank-transformed sGFAP and each sub-group was included to assess the inter-group differences.

Abbreviations: AQP4-IgG: aquaporin-4 immunoglobulin G; β: standardized estimate; CI: confidence interval; η_ρ^2: partial eta-squared; EDSS: Expanded Disability Status Scale; N: number of eyes; ON: optic neuritis; sGFAP: serum glial fibrillary acidic protein.

Table e-4. Association of sNfL age-adjusted Z-score with retinal layer thickness and foveal morphometry parameters in subgroups of AQP4-IgG$^+$ NMOSD subjects with EDSS ≤ 3 or > 3 and last attack within ≤ 1 year or > 1 year

		EDSS		**Time since last non-ON attack**	
		≤ 3.0 (N = 17)	> 3.0 (N = 17)	≤ 1 Year (N = 12)	> 1 Year (N = 22)
pRNFL thickness (μm)	β (95%CI)	-0.42 (-1.05 to 0.21)	-0.14 (-0.61 to 0.33)	-0.26 (-0.93 to 0.41)	-0.45 (-0.92 to 0.02)
	p-value	0.224	0.571	0.474	0.084
	η_ρ^2 for interaction with sNfL, *p*-value	$\eta_\rho^2 = 6.46e^{-3}$, $p = 0.713$		$\eta_\rho^2 = 4.86e^{-4}$, $p = 0.919$	
mRNFL thickness (μm)	β (95%CI)	-0.10 (-0.79 to 0.59)	-0.69 (-1.22 to -0.16)	-0.71 (-1.45 to 0.03)	-0.11 (-0.70 to 0.48)
	p-value	0.788	0.030	0.117	0.726
	η_ρ^2 for interaction with sNfL, *p*-value	$\eta_\rho^2 = 0.12$, $p = 0.124$		$\eta_\rho^2 = 0.08$, $p = 0.210$	
GCIPL thickness (μm)	β (95%CI)	-0.43 (-1.10 to 0.24)	-0.44 (-1.05 to 0.17)	-0.60 (-1.34 to 0.14)	-0.34 (-0.97 to 0.29)
	p-value	0.235	0.195	0.161	0.315
	η_ρ^2 for interaction with sNfL, *p*-value	$\eta_\rho^2 = 1.30e^{-5}$, $p = 0.988$		$\eta_\rho^2 = 0.06$, $p = 0.290$	
Average rim disk diameter (mm)	β (95%CI)	-0.45 (-1.06 to 0.16)	-0.18 (-0.75 to 0.39)	-0.58 (-1.17 to 0.01)	-0.22 (-0.75 to 0.31)

	p-value	0.186	0.551	0.105	0.432
	η_p^2 for interaction with sNfL, *p*-value	$\eta_p^2 = 0.05$, $p = 0.340$		$\eta_p^2 = 0.01$, $p = 0.604$	
Average slope disk diameter (mm)	β (95%CI)	0.40 (-0.21 to 1.01)	0.17 (-0.38 to 0.72)	0.06 (-0.70 to 0.82)	0.30 (-0.25 to 0.85)
	p-value	0.231	0.557	0.877	0.289
	η_p^2 for interaction with sNfL, *p*-value	$\eta_p^2 = 0.01$, $p = 0.648$		$\eta_p^2 = 0.02$, $p = 0.501$	
Average pit flat disk diameter (mm)	β (95%CI)	0.20 (-0.45 to 0.85)	0.18 (-0.43 to 0.79)	0.09 (-0.81 to 0.99)	0.24 (-0.31 to 0.79)
	p-value	0.561	0.580	0.857	0.460
	η_p^2 for interaction with sNfL, *p*-value	$\eta_p^2 = 6.35e^{-4}$, $p = 0.914$		$\eta_p^2 = 9.64e^{-3}$, $p = 0.675$	
Inner rim volume (mm^3)	β (95%CI)	-0.41 (-1.04 to 0.22)	-0.34 (-0.89 to 0.21)	-0.19 (-0.95 to 0.57)	-0.37 (-0.92 to 0.18)
	p-value	0.234	0.260	0.645	0.210
	η_p^2 for interaction with sNfL, *p*-value	$\eta_p^2 = 4.02e^{-4}$, $p = 0.931$		$\eta_p^2 = 0.02$, $p = 0.518$	
Rim volume (mm^3)	β (95%CI)	-0.59 (-1.14 to -0.04)	-0.35 (-0.92 to 0.22)	-0.63 (-1.20 to -0.06)	-0.38 (-0.89 to 0.13)
	p-value	0.066	0.255	0.074	0.171
	η_p^2 for interaction with sNfL, *p*-value	$\eta_p^2 = 0.06$, $p = 0.279$		$\eta_p^2 = 0.01$, $p = 0.663$	
Average pit depth (mm)	β (95%CI)	-0.55 (-1.08 to -0.02)	-0.23 (-0.84 to 0.38)	-0.47 (-1.20 to 0.26)	-0.30 (-0.79 to 0.19)
	p-value	0.074	0.483	0.256	0.252
	η_p^2 for interaction with sNfL, *p*-value	$\eta_p^2 = 0.02$, $p = 0.523$		$\eta_p^2 = 0.02$, $p = 0.590$	
Average rim height (mm)	β (95%CI)	-0.59 (-1.22 to 0.04)	-0.60 (-1.17 to -0.03)	-0.72 (-1.37 to -0.07)	-0.52 (-1.07 to 0.03)
	p-value	0.099	0.062	0.071	0.085

	η_ρ^2 for interaction with sNfL, *p*-value	$\eta_\rho^2 = 3.43e^{-3}$, $p = 0.803$		$\eta_\rho^2 = 0.02$, $p = 0.580$	
Central foveal thickness (mm)	β (95%CI)	-0.15 (-0.84 to 0.53)	-0.34 (-0.90 to 0.22)	-0.04 (-0.91 to 0.82)	-0.23 (-0.78 to 0.31)
	p-value	0.667	0.256	0.923	0.416
	η_ρ^2 for interaction with sNfL, *p*-value	$\eta_\rho^2 = 0.01$, $p = 0.648$		$\eta_\rho^2 = 0.01$, $p = 0.612$	

Analyzed with linear mixed effect model (dependent variables: OCT measures; independent fixed effect for sNfL age-adjusted Z-score; random intercepts for subjects) in 34 non-ON eyes from 25 AQP4-IgG$^+$ NMOSD patients. An interaction term of sNfL age-adjusted Z-score and each sub-group was included to assess the inter-group differences.

Abbreviations: AQP4-IgG: aquaporin-4 immunoglobulin G; β: standardized estimate; CI: confidence interval; η_ρ^2: partial eta-squared; EDSS: Expanded Disability Status Scale; GCIPL: combined macular ganglion cell and inner plexiform layer; mRNFL: macular retinal nerve fiber layer; N: number of eyes; ON: optic neuritis; pRNFL: peri-papillary retinal nerve fiber layer; sNfL: serum neurofilament light chain.

Table e-5. Association of sGFAP and sNfL with foveal morphometry parameters in AQP4-IgG$^+$ NMOSD subjects with or without a history of ON.

	Normalized rank-transformed sGFAP			**sNfL age-adjusted Z-score**		
		ON History			**ON History**	
		ON$^+$ (N = 22)	ON$^-$ (N = 34)		ON$^+$ (N = 22)	ON$^-$ (N = 34)
pRNFL thickness (μm)	β (95%CI)	-0.13 (-0.59 to 0.34)	-0.44 (-0.89 to 0.01)	β (95%CI)	0.04 (-0.40 to 0.48)	-0.31 (-0.67 to 0.04)
	p-value	0.604	0.065	*p*-value	0.868	0.095
	η_ρ^2 for interaction with sGFAP, *p*-value	$\eta_\rho^2 = 0.06$, $p = 0.071$		η_ρ^2 for interaction with sNfL, *p*-value	$\eta_\rho^2 = 0.02$, $p = 0.329$	
mRNFL thickness (μm)	β (95%CI)	-0.07 (-0.56 to 0.41)	-0.91 (-1.31 to -0.51)	β (95%CI)	-0.18 (-0.66 to 0.31)	-0.45 (-0.90 to 0.00)
	p-value	0.778	2.78 e^{-4}	*p*-value	0.485	0.060
	η_ρ^2 for interaction	$\eta_\rho^2 = 0.07$, $p = 0.060$		η_ρ^2 for interaction	$\eta_\rho^2 = 5.83e^{-4}$, $p = 0.868$	

	with sGFAP, *p*-value			with sNfL, *p*-value		
GCIPL thickness (µm)	β (95%CI)	-0.11 (-0.60 to 0.39)	-0.75 (-1.23 to -0.27)	β (95%CI)	-0.22 (-0.72 to 0.27)	-0.48 (-0.91 to -0.05)
	p-value	0.678	0.007	*p*-value	0.396	0.039
	η_ρ^2 for interaction with sGFAP, *p*-value	$\eta_\rho^2 = 0.11$, $p = 0.032$		η_ρ^2 for interaction with sNfL, *p*-value	$\eta_\rho^2 = 5.76e^{-3}$, $p = 0.622$	
Average rim disk diameter (mm)	β (95%CI)	0.08 (-0.41 to 0.56)	-0.55 (-0.96 to -0.14)	β (95%CI)	-0.20 (-0.65 to 0.25)	-0.40 (-0.77 to -0.02)
	p-value	0.767	0.019	*p*-value	0.405	0.052
	η_ρ^2 for interaction with sGFAP, *p*-value	$\eta_\rho^2 = 0.11$, $p = 0.074$		η_ρ^2 for interaction with sNfL, *p*-value	$\eta_\rho^2 = 0.05$, $p = 0.227$	
Average slope disk diameter (mm)	β (95%CI)	0.11 (-0.37 to 0.60)	-0.19 (-0.70 to 0.32)	β (95%CI)	-0.15 (-0.63 to 0.32)	0.18 (-0.23 to 0.59)
	p-value	0.648	0.469	*p*-value	0.530	0.402
	η_ρ^2 for interaction with sGFAP, *p*-value	$\eta_\rho^2 = 6.77e^{-3}$, $p = 0.667$		η_ρ^2 for interaction with sNfL, *p*-value	$\eta_\rho^2 = 0.01$, $p = 0.566$	
Average pit flat disk diameter (mm)	β (95%CI)	-0.01 (-0.53 to 0.52)	0.05 (-0.50 to 0.60)	β (95%CI)	-0.02 (-0.52 to 0.49)	0.21 (-0.24 to 0.66)
	p-value	0.978	0.874	*p*-value	0.943	0.368
	η_ρ^2 for interaction with sGFAP, *p*-value	$\eta_\rho^2 = 0.01$, $p = 0.547$		η_ρ^2 for interaction with sNfL, *p*-value	$\eta_\rho^2 = 0.03$, $p = 0.326$	
Inner rim volume (mm^3)	β (95%CI)	-0.06 (-0.55 to 0.43)	0.02 (-0.51 to 0.55)	β (95%CI)	0.09 (-0.39 to 0.56)	-0.26 (-0.69 to 0.17)
	p-value	0.813	0.932	*p*-value	0.729	0.234
	η_ρ^2 for interaction with sGFAP, *p*-value	$\eta_\rho^2 = 7.81e^{-3}$, $p = 0.633$		η_ρ^2 for interaction with sNfL, *p*-value	$\eta_\rho^2 = 2.54e^{-3}$, $p = 0.786$	
Rim volume (mm^3)	β (95%CI)	0.04 (-0.45 to 0.53)	-0.60 (-1.01 to -0.19)	β (95%CI)	-0.14 (-0.61 to -0.33)	-0.52 (-0.87 to -0.17)
	p-value	0.876	0.011	*p*-value	0.577	0.010
	η_ρ^2 for interaction with sGFAP, *p*-value	$\eta_\rho^2 = 0.13$, $p = 0.042$		η_ρ^2 for interaction with sNfL, *p*-value	$\eta_\rho^2 = 0.05$, $p = 0.210$	
Average pit depth (mm)	β (95%CI)	0.06 (-0.47 to 0.58)	-0.59 (-0.63 to -0.55)	β (95%CI)	-0.23 (-0.71 to 0.25)	-0.45 (-0.84 to -0.06)
	p-value	0.832	0.020	*p*-value	0.357	0.034

	η_ρ^2 for interaction with sGFAP, *p*-value	$\eta_\rho^2 = 0.14$, $p = 0.046$		η_ρ^2 for interaction with sNfL, *p*-value	$\eta_\rho^2 = 3.09e^{-4}$, $p = 0.926$	
Average rim height (mm)	β (95%CI)	0.06 (-0.46 to 0.58)	-0.79 (-1.24 to -0.34)	β (95%CI)	-0.14 (-0.64 to 0.35)	-0.63 (-1.02 to -0.24)
	p-value	0.819	0.003	*p*-value	0.575	0.004
	η_ρ^2 for interaction with sGFAP, *p*-value	$\eta_\rho^2 = 0.16$, $p = 0.013$		η_ρ^2 for interaction with sNfL, *p*-value	$\eta_\rho^2 = 0.02$, $p = 0.394$	
Central foveal thickness (mm)	β (95%CI)	-0.04 (-0.54 to 0.47)	0.11 (-0.42 to 0.64)	β (95%CI)	0.17 (-0.29 to 0.63)	-0.05 (-0.50 to 0.40)
	p-value	0.889	0.690	*p*-value	0.486	0.838
	η_ρ^2 for interaction with sGFAP, *p*-value	$\eta_\rho^2 = 0.02$, $p = 0.478$		η_ρ^2 for interaction with sNfL, *p*-value	$\eta_\rho^2 = 0.03$, $p = 0.329$	

Analyzed with linear mixed effect model (dependent variables: OCT measures; independent fixed effect for normalized rank-transformed sGFAP and age or sNfL age-adjusted Z-score; random intercepts for subjects) in 56 eyes from 33 AQP4-IgG$^+$ NMOSD patients. An interaction term of normalized rank-transformed sGFAP or sNfL age-adjusted Z-score and each sub-group was included to assess the inter-group differences.

Abbreviations: AQP4-IgG: aquaporin-4 immunoglobulin G; β: standardized estimate; CI: confidence interval; η_ρ^2: partial eta-squared; GCIPL: combined macular ganglion cell and inner plexiform layer; mRNFL: macular retinal nerve fiber layer; N: number of eyes; ON: optic neuritis; pRNFL: peri-papillary retinal nerve fiber layer; sGFAP: serum glial fibrillary acidic protein; sNfL: serum neurofilament light chain.

Figure e-1. Non-ON eyes selection for OCT analyses in AQP4-IgG$^+$ NMOSD and MOGAD patients

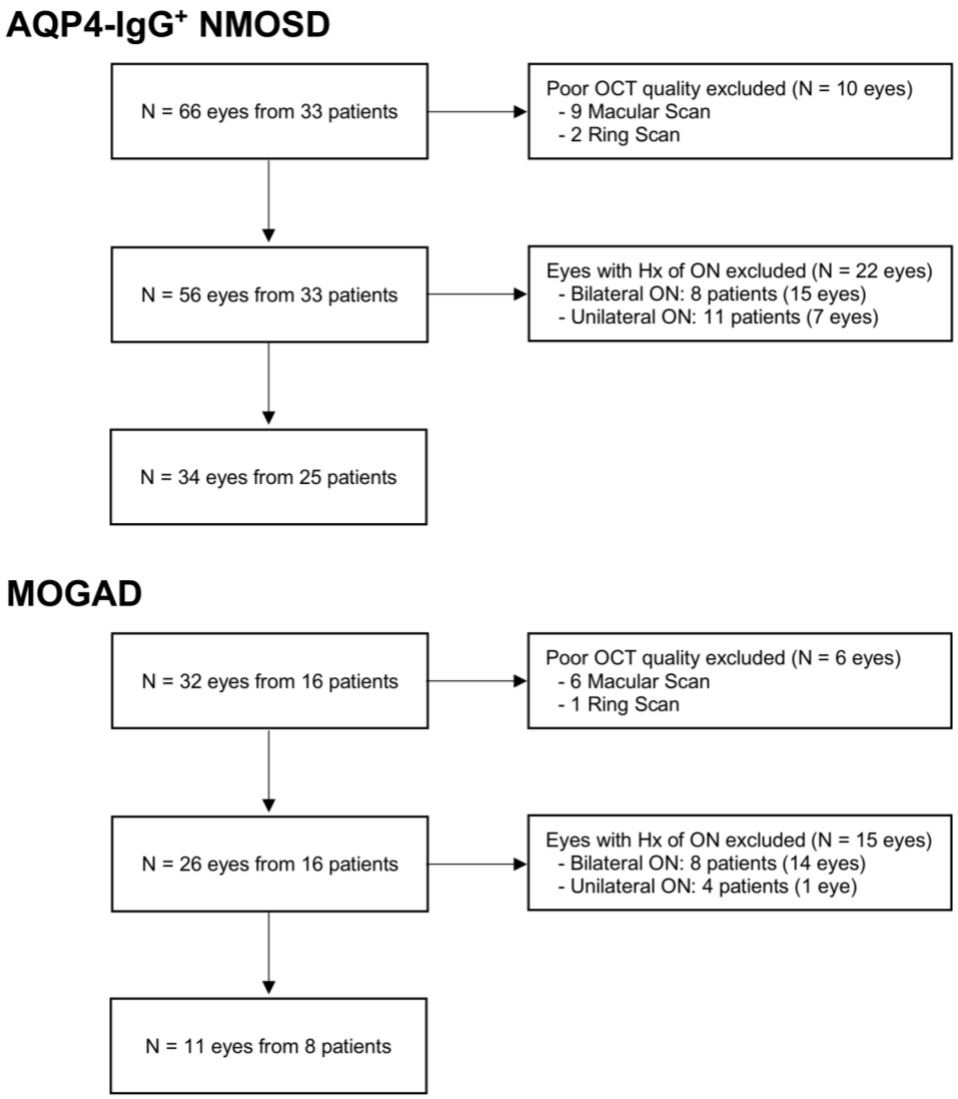

Abbreviations: AQP4-IgG: aquaporin-4 immunoglobulin G; MOGAD: myelin oligodendrocyte glycoprotein antibody associated disorders; NMOSD: Neuromyelitis optica spectrum disorder; OCT: optical coherence tomography; ON: optic neuritis.

Statistical software references

R version 4.0.2 was used, with the following packages: tableone, lme4, lmerTest, MuMIn, ggplot2, ggpubr, and effectsize packages.

(1) Yoshida K, Bartel A (2022). tableone: Create 'Table 1' to Describe Baseline Characteristics with or without Propensity Score Weights. R package version 0.13.2. https://CRAN.R-project.org/package=tableone.

(2) Douglas B, Martin M, Ben B, Steve W (2015). Fitting Linear Mixed-Effects Models Using lme4. Journal of Statistical Software, 67(1), 1-48. doi:10.18637/jss.v067.i01.

(3) Kuznetsova A, Brockhoff PB, Christensen RHB (2017). lmerTest Package: Tests in Linear Mixed Effects Models. Journal of Statistical Software, 82 (13), 1-26. doi:10.18637/jss.v082.i13.

(4) Bartoń K (2022). MuMIn: Multi-Model Inference. R package version 1.46.0. https://CRAN.R-project.org/package=MuMIn.

(5) H. Wickham. ggplot2: Elegant Graphics for Data Analysis. Springer-Verlag New York, 2016.

(6) Kassambara A (2020). ggpubr: 'ggplot2' Based Publication Ready Plots. R package version 0.4.0. https://CRAN.R-project.org/package=ggpubr.

(7) Ben-Shachar M, Lüdecke D, Makowski D (2020). effectsize: Estimation of Effect Size Indices and Standardized Parameters. Journal of Open Source Software, 5(56), 2815. doi: 10.21105/joss.02815

Acknowledgements

We thank Charlotte Bereuter and Carla Leutloff for excellent technical support. S.J. is grateful to Anna Eschlbeck, Katharina Mattes, and the staff of the Nikon Imaging Center at the University of Heidelberg, Heidelberg, Germany, for excellent technical support. We thank all patients for participation in this study.

Conflict of interest

1. T.-Y. Lin, P. Schindler, U. Grittner, A. Lu, A.S. Duchow, S. Jarius, J. Kuhle, P. Benkert and T. Schmitz-Hübsch report no relevant disclosures.
2. F.C. Oertel was an employee of Nocturne GmbH and receives research support by the American Academy of Neurology, the National Multiple Sclerosis Society and Deutsche Gesellschaft für Neurologie (*German Neurology Society*), unrelated to this work.
3. S. Motamedi is named as co-inventor on the patent application for the foveal shape analysis method used by this manuscript ("Method for estimating shape parameters of the fovea by optical coherence tomography", International Publication Number: "WO 2019/016319 A1").
4. S.K. Yadav is named as co-inventor on the patent application for the foveal shape analysis method used by this manuscript ("Method for estimating shape parameters of the fovea by optical coherence tomography", International Publication Number: "WO 2019/016319 A1") and a cofounder of medical technology companies Nocturne GmbH.
5. A.U. Brandt is cofounder and shareholder of medical technology companies Nocturne GmbH and Motognosis GmbH. He is named as inventor on several patent applications describing MS biomarkers, visual perceptive computing based motor function analysis, and retinal image analysis.
6. J. Bellmann-Strobl has received speaking honoraria and travel grants from Bayer Healthcare, and sanofi-aventis/Genzyme, in addition received compensation for serving on a scientific advisory board of Roche, unrelated to the presented work.
7. F. Paul served on the scientific advisory boards of Novartis and MedImmune; received travel funding

and/or speaker honoraria from Bayer, Novartis, Biogen, Teva, Sanofi-Aventis/Genzyme, Merck Serono, Alexion, Chugai, MedImmune, and Shire; is an associate editor of *Neurology: Neuroimmunology & Neuroinflammation*; is an academic editor of *PLoS ONE*; consulted for Sanofi Genzyme, Biogen, MedImmune, Shire, and Alexion; received research support from Bayer, Novartis, Biogen, Teva, Sanofi-Aventis/Geynzme, Alexion, and Merck Serono; and received research support from the German Research Council, Werth Stiftung of the City of Cologne, German Ministry of Education and Research, Arthur Arnstein Stiftung Berlin, EU FP7 Framework Program, Arthur Arnstein Foundation Berlin, Guthy-Jackson Charitable Foundation, and NMSS.

8. K. Ruprecht received research support from Novartis, Merck Serono, German Ministry of Education and Research, European Union (821283-2), Stiftung Charité (BIH Clinical Fellow Program) and Arthur Arnstein Foundation; received travel grants from Guthy-Jackson Charitable Foundation.
9. H.G. Zimmermann received research grants from Novartis and speaking honoraria from Bayer Healthcare and Novartis.

References

1. Jarius S, Paul F, Weinshenker BG, Levy M, Kim HJ, Wildemann B. Neuromyelitis optica. Nat Rev Dis Prim. 2020;6:85.
2. Marignier R, Hacohen Y, Cobo-Calvo A, et al. Myelin-oligodendrocyte glycoprotein antibody-associated disease. Lancet Neurol. 2021;20:762–772.
3. Jarius S, Ruprecht K, Kleiter I, et al. MOG-IgG in NMO and related disorders: A multicenter study of 50 patients. Part 2: Epidemiology, clinical presentation, radiological and laboratory features, treatment responses, and long-term outcome. J Neuroinflammation. 2016;13:1–45.
4. Wingerchuk DM, Zhang I, Kielhorn A, et al. Network Meta-analysis of Food and Drug Administration-approved Treatment Options for Adults with Aquaporin-4 Immunoglobulin G-positive Neuromyelitis Optica Spectrum Disorder. Neurol Ther. 2021;11:123–135.
5. Wingerchuk DM, Banwell B, Bennett JL, et al. International consensus diagnostic criteria for neuromyelitis optica spectrum disorders. Neurology. 2015;85:177–189.
6. Pache F, Zimmermann H, Mikolajczak J, et al. MOG-IgG in NMO and related disorders: A multicenter study of 50 patients. Part 4: Afferent visual system damage after optic neuritis in MOG-IgG-seropositive versus AQP4-IgG-seropositive patients. J Neuroinflammation. 2016;13:1–10.
7. Vabanesi M, Pisa M, Guerrieri S, et al. In vivo structural and functional assessment of optic nerve damage in neuromyelitis optica spectrum disorders and multiple sclerosis. Sci Rep. 2019;9:10371.
8. Lin TY, Chien C, Lu A, Paul F, Zimmermann HG. Retinal optical coherence tomography and magnetic resonance imaging in neuromyelitis optica spectrum disorders and MOG-antibody associated disorders: an updated review. Expert Rev Neurother. 2021;21:1101–1123.
9. Motamedi S, Oertel FC, Yadav SK, et al. Altered fovea in AQP4-IgG-seropositive neuromyelitis optica spectrum disorders. Neurol Neuroimmunol neuroinflammation. 2020;7:e805.
10. Filippatou AG, Vasileiou ES, He Y, et al. Evidence of subclinical quantitative retinal layer abnormalities in AQP4-IgG seropositive NMOSD. Mult Scler J. 2021;27:1738–1748.

11. Oertel FC, Havla J, Roca-Fernández A, et al. Retinal ganglion cell loss in neuromyelitis optica: A longitudinal study. J Neurol Neurosurg Psychiatry. 2018;89:1259–1265.
12. Middeldorp J, Hol EM. GFAP in health and disease. Prog Neurobiol. 2011;93:421–443.
13. Watanabe M, Nakamura Y, Michalak Z, et al. Serum GFAP and neurofilament light as biomarkers of disease activity and disability in NMOSD. Neurology. 2019;93:e1299–e1311.
14. Kim H, Lee EJ, Kim S, et al. Serum biomarkers in myelin oligodendrocyte glycoprotein antibody-associated disease. Neurol Neuroimmunol neuroinflammation. 2020;7:e708.
15. Schindler P, Grittner U, Oechtering J, et al. Serum GFAP and NfL as disease severity and prognostic biomarkers in patients with aquaporin-4 antibody-positive neuromyelitis optica spectrum disorder. J Neuroinflammation. 2021;18:105.
16. Aktas O, Smith MA, Rees WA, et al. Serum Glial Fibrillary Acidic Protein: A Neuromyelitis Optica Spectrum Disorder Biomarker. Ann Neurol. 2021;89:895–910.
17. Aly L, Strauß EM, Feucht N, et al. Optical coherence tomography angiography indicates subclinical retinal disease in neuromyelitis optica spectrum disorders. Mult Scler J. Epub 2021.:13524585211028832.
18. Jarius S, Paul F, Aktas O, et al. MOG encephalomyelitis: International recommendations on diagnosis and antibody testing. J Neuroinflammation. 2018;15:134.
19. Jarius S, Probst C, Borowski K, et al. Standardized method for the detection of antibodies to aquaporin-4 based on a highly sensitive immunofluorescence assay employing recombinant target antigen. J Neurol Sci. 2010;291:52–56.
20. Jarius S, Ruprecht K, Kleiter I, et al. MOG-IgG in NMO and related disorders: A multicenter study of 50 patients. Part 1: Frequency, syndrome specificity, influence of disease activity, long-term course, association with AQP4-IgG, and origin. J Neuroinflammation. 2016;13:279.
21. Disanto G, Barro C, Benkert P, et al. Serum Neurofilament light: A biomarker of neuronal damage in multiple sclerosis. Ann Neurol. 2017;81:857–870.
22. Schippling S, Balk LJ, Costello F, et al. Quality control for retinal OCT in multiple sclerosis:

608 Validation of the OSCAR-IB criteria. Mult Scler J. 2015;21:163–170.
609 23. Aytulun A, Cruz-Herranz A, Aktas O, et al. The APOSTEL 2.0 Recommendations for Reporting
610 Quantitative Optical Coherence Tomography Studies. Neurology. 2021;97:68–79.
611 24. Yadav SK, Motamedi S, Oberwahrenbrock T, et al. CuBe: parametric modeling of 3D foveal shape
612 using cubic Bézier. Biomed Opt Express. 2017;8:4181.
613 25. Odom JV, Bach M, Brigell M, et al. ISCEV standard for clinical visual evoked potentials: (2016
614 update). Doc Ophthalmol. 2016;133:1–9.
615 26. Barro C, Benkert P, Disanto G, et al. Serum neurofilament as a predictor of disease worsening and
616 brain and spinal cord atrophy in multiple sclerosis. Brain. 2018;141:2382–2391.
617 27. Roca-Fernández A, Oertel FC, Yeo T, et al. Foveal changes in aquaporin-4 antibody seropositive
618 neuromyelitis optica spectrum disorder are independent of optic neuritis and not overtly
619 progressive. Eur J Neurol. 2021;28:2280–2293.
620 28. Molazadeh N, Filippatou AG, Vasileiou ES, Levy M, Sotirchos ES. Evidence for and against
621 subclinical disease activity and progressive disease in MOG antibody disease and neuromyelitis
622 optica spectrum disorder. J Neuroimmunol. 2021;360:577702.
623 29. Takano R, Misu T, Takahashi T, Sato S, Fujihara K, Itoyama Y. Astrocytic damage is far more
624 severe than demyelination in NMO: A clinical CSF biomarker study. Neurology. 2010;75:208–
625 216.
626 30. Abboud H, Petrak A, Mealy M, Sasidharan S, Siddique L, Levy M. Treatment of acute relapses in
627 neuromyelitis optica: Steroids alone versus steroids plus plasma exchange. Mult Scler.
628 2016;22:185–192.
629 31. Ringelstein M, Harmel J, Zimmermann H, et al. Longitudinal optic neuritis-unrelated visual
630 evoked potential changes in NMO spectrum disorders. Neurology. 2020;94:e407–e418.
631 32. Tian DC, Su L, Fan M, et al. Bidirectional degeneration in the visual pathway in neuromyelitis
632 optica spectrum. Mult Scler J. 2018;24:1585–1593.
633 33. Lundkvist A, Reichenbach A, Betsholtz C, Carmeliet P, Wolburg H, Pekny M. Under stress, the

absence of intermediate filaments from Müller cells in the retina has structural and functional consequences. J Cell Sci. 2004;117:3481–3488.

34. Verardo MR, Lewis GP, Takeda M, et al. Abnormal reactivity of Müller cells after retinal detachment in mice deficient in GFAP and vimentin. Investig Ophthalmol Vis Sci. 2008;49:3659–3665.

35. Oertel FC, Specovius S, Zimmermann HG, et al. Retinal optical coherence tomography in neuromyelitis optica. Neurol Neuroimmunol neuroinflammation. 2021;8:e1068.

36. Hyun J-W, Kim Y, Kim KH, et al. CSF GFAP levels in double seronegative neuromyelitis optica spectrum disorder: no evidence of astrocyte damage. J Neuroinflammation. 2022;19:86.